Colloids and Surfaces A: Physicochemical and Engineering Aspects 692 (2024) 133899

Contents lists available at ScienceDirect

Colloids and Surfaces A: Physicochemical and Engineering Aspects

journal homepage: www.elsevier.com/locate/colsurfa

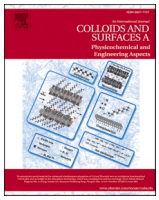

Box-Behnken design for the synthesis optimization of mesoporous sulfur-doped carbon-based materials from birch waste: Promising candidates for environmental and energy storage application

Ewen Laisné [a,b,1], Julie Thivet [a,c,1], Gopinathan Manavalan [a,d], Shaikshavali Petnikota [a], Jyri-Pekka Mikkola [d,e], Mikael Thyrel [a], Tao Hu [f], Eder Claudio Lima [g], Mu. Naushad [h], Ulla Lassi [f], Glaydson Simoes dos Reis [a,*]

[a] Department of Forest Biomaterials and Technology, Biomass Technology Centre, Swedish University of Agricultural Sciences, Umeå SE-901 83, Sweden
[b] IMT Mines Albi-Carmaux, Albi 81000, France
[c] Ecole Nationale Supérieure de Chimie de Montpellier, Montpellier, France
[d] Wallenberg Wood Science Center, Technical Chemistry, Department of Chemistry, Umeå University, Umeå 90187, Sweden
[e] Industrial Chemistry and Reaction Engineering, Johan Gadolin Process Chemistry Centre, Åbo Akademi University, Åbo-Turku 20500, Finland
[f] Research Unit of Sustainable Chemistry, University of Oulu, P.O. Box 3000, Oulu FI-90014, Finland
[g] Institute of Chemistry, Federal University of Rio Grand do Sul (UFRGS), Porto Alegre, RS, Brazil
[h] Department of Chemistry, College of Science, King Saud University, P.O. Box 2455, Riyadh-11451, Saudi Arabia

GRAPHICAL ABSTRACT

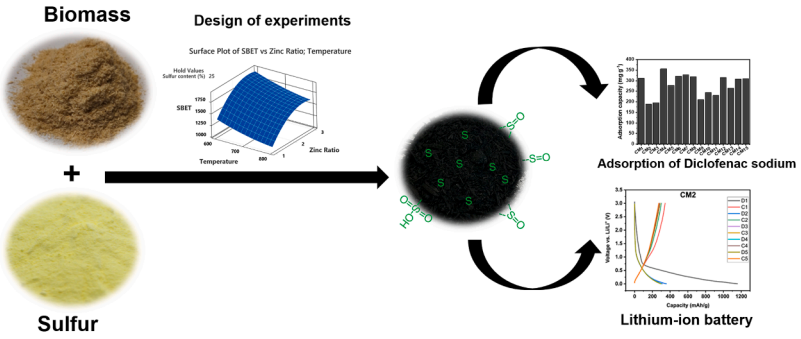

ARTICLE INFO

Keywords:
Birch residues
Sulfur doping
Sulfur-doped carbons
Adsorption of sodium diclofenac
Lithium ion battery

ABSTRACT

The development of biomass-based carbon materials has accelerated the research interest in environmental (e.g., adsorbents for wastewater decontamination) and energy applications (e.g., batteries). In this paper, we developed a series of carbon materials (CMs) using a sulfur doping strategy to improve the physicochemical, adsorptive and energy storage properties of the aforementioned CMs. CMs were prepared and optimized using an experimental design denoted as the Box-Behnken design approach with three independent factors (i.e., the temperature of pyrolysis, zinc chloride: biomass ratio and sulfur: biomass ratio), and the responses were

* Corresponding author.
E-mail address: glaydson.simoes.dos.reis@slu.se (G.S. dos Reis).
[1] These authors contributed equally

https://doi.org/10.1016/j.colsurfa.2024.133899
Received 24 January 2024; Received in revised form 17 March 2024; Accepted 2 April 2024
Available online 3 April 2024

evaluated, namely the Specific Surface Area (S_{BET}), mesopore area (A_{Meso}) and micropore area (A_{Micro}) with the help of Nitrogen Physisorption. According to the statistical analysis, under the studied conditions, the responses were mainly influenced by the pyrolysis temperature and $ZnCl_2$ ratio, while the sulfur content did not give rise to any remarkable differences in the selected responses. The physicochemical characterization of the CMs suggested that very high Specific Surface Areas ranging from 1069 to 1925 $m^2\ g^{-1}$ were obtained. The sulfur doping resulted in up to 7.33 wt% of sulfur in the CM structure, which yielded CMs with more defects and hydrophilic surfaces. When tested as adsorbents, CMs exhibited a very high adsorption capacity (190 – 356 mg g^{-1}), and as anodes, they demonstrated a competitive Lithium Ion Battery (LIB) storage capacity, at least during the first five cycles (306 $mAhg^{-1}$ at 1 C for CM9). However, further studies on long-term cyclability are required to prove the CM materials suitability in LIBs. This work extends our understanding of how pyrolysis and sulfur doping of biomass feedstock affects carbon materials' usability, final characteristics and potential to use in wastewater decontamination by adsorption and as anodes in LIBs.

1. Introduction

Residual biomass is no longer a waste; it is a valuable raw material that can be used to prepare many high-value products [1,2]. One good alternative use of residual biomass is to prepare materials with well-developed porosity and high surface area (activated carbon-AC, biochars-BC, and other carbon-based materials-CM) [3–6]. CMs are typically prepared by pyrolysis via physical or chemical activation in the absence of oxygen [3–6]. Thanks to the CMs' intrinsic properties, such as high surface area, engineered pore networks, and surface functionalities, they are widely employed as adsorbents to remove pollutants from wastewater [2–4] and as electrode materials in energy storage systems [4–7]. Sustainable CM can be produced from any kind of biomass (from animal or plant biomass), generally at temperatures higher than 500 °C. Moreover, to improve the physicochemical properties of the CMs, a chemical or physical activation is required to yield CMs with suitable properties for the desired application. For instance, Xue *et al.*, [8] modified a porous carbon with Co_2NiSe_4 using a combination of hydrothermal carbonization and pyrolysis, and employed it as efficient electrodes in advanced energy storage systems. It was found that both the thermal and chemical treatment greatly enhanced the electrochemical properties of the materials. The properties of the CMs widely differ depending on the various parameters applied during the pyrolysis and activation processes, respectively, and, for instance, temperature, heating rate, and holding time [5,9], and the chosen activation process, the biomass/activator ratio as well as the activation method: physical or chemical [9–11].

All aforementioned factors greatly influence the CMs properties, and often they act concomitantly [5,12]. Therefore, it is highly complex to determine to which degree, but also how, these variables influence the CMs fabrication process and thus the resulting properties. Therefore, identifying which and how these factors influence CM properties is crucial upon optimizing its production process. The Design of Experiment (DoE) method enables to study these variables' simultaneous influence in a given single experiment [5,12,13]. This methodology provides a means to optimize the number of experiments to recover significant data and save resources and time by evaluating the factors most influential in the CMs preparation [5,12,13].

In scientific literature, it is abundant to employ the DoE approach to prepare CMs by using biomass precursors such as spruce bark [5], cabbage waste [14], conifer brash [15], coconut shell [16] etc. The optimized preparation parameters of these CMs have been successfully identified thanks to the DoE evaluation, e.g., Jarmal *et al.* [17] employed a DoE to evaluate the CMs preparation from Scottish wood, studying two process parameters (activation CO_2 flow rate ranging from 100 mL/min to 250 mL/min and pyrolysis time ranging from 20 min to 100 min). They evaluated the influence of these factors on two responses (specific surface area and the yield). The optimized parameters were found for the CMs with the highest surface area of 764 m^2/g and a yield of 15% at 60 minutes of pyrolysis time. Nevertheless, the gas flow appeared not to influence these two responses in a significant way. In another work, dos Reis *et al.* [5], using spruce bark as a biomass precursor to produce CMs, evaluated the influence of parameters such as the pyrolysis temperature (from 700 to 900 °C), pyrolysis reaction time (1 – 3 h), and the ratio (in mass) of biomass-to-chemical activator ($ZnCl_2$, ranging from 0.5 to 1.5 in weight) on the specific surface area as a response; It was found that the residence time, the amount of $ZnCl_2$ and temperature were the most influential factors and the highest surface area value was reached under the pyrolysis conditions of 700 °C, 1 h, and 1.0:1.5 (wt:wt). The aforementioned results show that the DoE approach is indeed an efficient tool to evaluate and optimize the CMs preparation when several parameters influence the preparation and, consequently, the resulting properties.

In this work, Silver birch waste (BW), also known as *Betula pendula,* was used as a biomass source to produce CMs with high-quality properties. In Sweden and, in general, in the Nordic countries, birch grows by 15 million m^3 annually and is harvested and utilized for industrial purposes. During birch wood processing, 12% of the tree mass is generated as bark [18,19] and is of low industrial value. Currently, most birch bark in Sweden is used for energy production. Birch waste is a good precursor candidate in CMs preparation due to its high lignin (27.9%) and holocellulose (49.8%) content [18,19]. CMs with different physicochemical properties can be readily produced from birch bark, resulting in carbon materials with multi-functional properties, including adsorptive and energy storage systems [20]. Moreover, heteroatom doping can further improve the physicochemical properties of CMs. Typical heteroatoms are nitrogen, boron, phosphorus, and sulfur [21,22]. Besides this, non-metal heteroatoms as CMs dopants are more sustainable, low-cost, and environment-friendly compared to toxic metals [21,22].

Sulfur is one of the most employed heteroatoms in CMs modification. The sufur electronegativity is 2.58, being close to that of carbon (2.55). Using S as a dopant can reduce the energy gap between the molecular orbitals, form thiophene groups, and enhance the reactivity of the catalysts to electron acceptors [23]. Moreover, introducing the S atom would adjust the spin density and polarizability of the S-doped CMs and increase the structural defects of carbon materials and their carbon layers. Also, these reaction sites may increase adsorptive properties and ion storage capacity in energy storage devices [23]. In addition, using of S is a promising strategy to produce doped CMs because of its large reserves, low cost, and environmental friendliness compared to transition metals.

Herein, we employed Birch waste to synthesize S-doped carbon materials using DoE to optimize the best preparation conditions to yield CMs with elevated Specific Surface Areas (S_{BET}) with a high mesopore area (A_{meso}). CMs were prepared through a chemical activation procedure using $ZnCl_2$ as an activating agent, widely known as an efficient reagent for mesoporosity development that is a highly desired property in applications related to solid-liquid separation and energy storage applications. This research brings an attractive, sustainable, and greener approach to produce suitable CMs that can purify polluted waters and are good electrode candidates. The current knowledge still has essential gaps to be filled by answering questions related to the preparation of CMs sourced from different biomass materials *versus* CM preparation methods and the optimal conditions, as well as the influence of the

Table 1
The textural characteristics of CMs under different synthesis conditions.

Samples	Temp.	Zinc Ratio	Sufur content (wt%)	S_{BET} (m^2 g^{-1})	A_{Meso} (m^2 g^{-1})	A_{Micro} (m^2 g^{-1})	S_{Meso} % (%)
CM1	600	1	25	1387	835	552	60.2
CM2	800	1	25	1069	404	665	37.8
CM3	600	3	25	1925	1822	103	94.6
CM4	800	3	25	1592	1390	202	87.3
CM5	600	2	0	1837	1705	132	92.8
CM6	800	2	0	1638	1349	289	82.4
CM7	600	2	50	1809	1309	500	72.4
CM8	800	2	50	1555	1190	365	76.5
CM9	700	1	0	1211	588	623	48.6
CM10	700	3	0	1515	1462	53	96.5
CM11	700	1	50	1232	478	754	38.8
CM12	700	3	50	1906	1887	19	99.0
CM13	700	2	25	1585	1296	289	81.8
CM14	700	2	25	1758	1584	174	90.1
CM15	700	2	25	1637	1550	87	94.7

doping techniques and how all these aspects are acting concomitantly to yield CMs with suitable physicochemical and adsorptive properties. Thus, we expect that this research can contribute to reducing the gaps and give a better understanding of the CMs properties related to the influence of the pyrolysis/activation and doping processes.

2. Materials and methods

2.1. CM preparation

The Birch Wood (BW) samples used in this study were obtained and processed at the SLU (Swedish University of Agricultural Sciences) Biomass Technology Center, Umeå, Sweden. The samples were ground into particle sizes under 0.5 mm, dried and used as such. Based on our earlier studies [3–5], a one-step pyrolysis/activation/doping was performed to prepare the CMs. 15.0 g of BW was mixed with the desired amounts of $ZnCl_2$ and sufur (as shown in Table 1). Next, approximately 20 mL of distilled water was added to the mixture to obtain a homogenous paste [3–5]. The paste was then dried in an oven at 75°C for 24 h and, consequently, placed in a metallic-crucible to be heated in a conventional high-temperature oven at a fixed heating rate of 10°C.min^{-1}, under a nitrogen flow of 50 mL. min^{-1}. The final pyrolysis temperature varied according to the DoE setup (shown in Table 1). Once the setup temperature was attained, it was held constant for 1 hour, then the oven was shut off to cool down under nitrogen flow. Afterwards, the CMs were then milled into a diameter of 200 μm and washed with 5 M HCl under reflux at 80°C for 2 hours to remove the remaining $ZnCl_2$ from the carbon matrix. Finally, the CMs were rinsed excessively with boiled distilled water until the pH of the washing water was observed to have a constant pH value (near pH 5), and then the CMs were dried at 75°C for 24 h before being stored for later use.

2.2. Experimental design

The Box-Behnken design (BBD) was used to perform the birch pyrolysis and activation. The BBD is made of incomplete block designs from a minimum of three factors. Each block comprises four combinations of the three factors: one is always at the central point, and the others vary from the lower (-1) to the upper (+1) limits. We chose to use the pyrolysis temperature (°C), Zinc Chloride/birch dry matter ratio (-), and Sulfur/birch dry matter ratio (-) as the most important factors in the experimental design, which was made of 15 experiments with three centre points and 12 factorial points (see Table S1). The upper and lower limits were determined by referring to the literature.

The B.E.T. (Brunauer-Emmet- Teller) surface area, S_{BET} (m^2g^{-1}); micropore surface area, S_{MICRO} (m^2g^{-1}); mesopore surface area and S_{MESO} (m^2g^{-1}); pore volume (cm^3g^{-1}) were selected as the responses (see Table S1). The influence of the factors on the responses (S_{BET}, A_{MICRO}, A_{MESO}) and the optimal values were calculated on the Minitab™ software.

2.3. CMs characterization

The porosity data from nitrogen isotherms were obtained based on the standard procedures [5,7]. The SSA values were obtained based on Brunauer–Emmett–Teller (B.E.T.) method, while the pore size distribution curves were obtained from Barrett–Joyner–Halenda (BJH) method. The elemental composition of the carbon materials was performed and obtained from a device analyzer (EA-IsoLink, Thermo Fisher Scientific). Briefly, oven-dried samples (0.05 g) were used to determine the contents of C, O, H, and S. Raman spectra were obtained using a Bruker Bravo spectrometer (Bruker, Ettlingen, Germany). The spectra were obtained by scanning from 800–2000 cm^{-1} (254 scans at 4 cm^{-1} resolution). Hydrophobic-hydrophilic index (HI) for the carbon materials were determined according to the methodology proposed in ref. [5]. X-ray photoelectron spectroscopy (XPS) analysis used a Thermo Fisher Scientific ESCALAB 250Xi XPS System. Measurements were done according to standard measuring procedures [5,7].

2.4. Preliminary adsorption tests

In order to test the ability of the CM to adsorb a targeted contaminant, all fifteen CMs were employed in the adsorption of sodium diclofenac (DCF) solution. In 50 mL Falcon tubes, 30 mg of CMs were introduced with 20 mL of DCF solution at an initial concentration of 700 $mg.L^{-1}$. The tubes were agitated in a shaker model TE-240 at 300 rpm for 3 h. Then, the samples were centrifuged to separate the two phases, solid and liquid properly. The liquid phase was recovered to quantify the remaining amount of DCF left after the adsorption employing a Shimadzu UV–visible spectrophotometer (model 1800) at λ_{max} of 276 nm. The adsorption capacity of the CMs was calculated based on Eq. (1):

$$q = \frac{(C_0 - C_f)}{m}.V$$

2.5. Preliminary battery tests

Electrode slurries of all the birch samples were made by mixing their powders, carbon black Super-P (Alfa Aesar) and PVDF binder (MTI Corporation) in 80:10:10 wt%, respectively, in a NMP (Sigma Aldrich) solvent. The as prepared slurries were coated onto a 10 μm thick Cu foil using the doctor-blade technique. After overnight drying at 80 ℃, the coated foils were punched into disks of 16 mm diameter. Fabricated birch electrodes were used as anodes to assemble coin cells (CR2032) using Li foil (0.6 mm thick, MSE Supplies) as the counter electrode. A 1.0 M $LiPF_6$ EC/DMC (1:1 v/v; Sigma Aldrich) was used as the electrolyte, whilst Whatman glass microfiber filters were used as separators. The coin-cell assembly was carried out inside an Ar-filled glove box (MBraun LABstar). All the cells were relaxed overnight before starting the measurements. The charge-discharge (galvanostatic cycling) measurements were carried out with a BioLogic BSC-805 battery cycler. All the coin-cells were tested at room temperature at 0.1 C (1 C = 372 mA/g) rate and in a voltage window of 0.005 – 3.0 V.

3. Results and discussion

3.1. Porosity data and Yield of the CMs

Porosity characteristics such specific surface area and pore size structure are important characteristics that play a crucial role on the adsorptive and electrochemical performances of any carbon materials

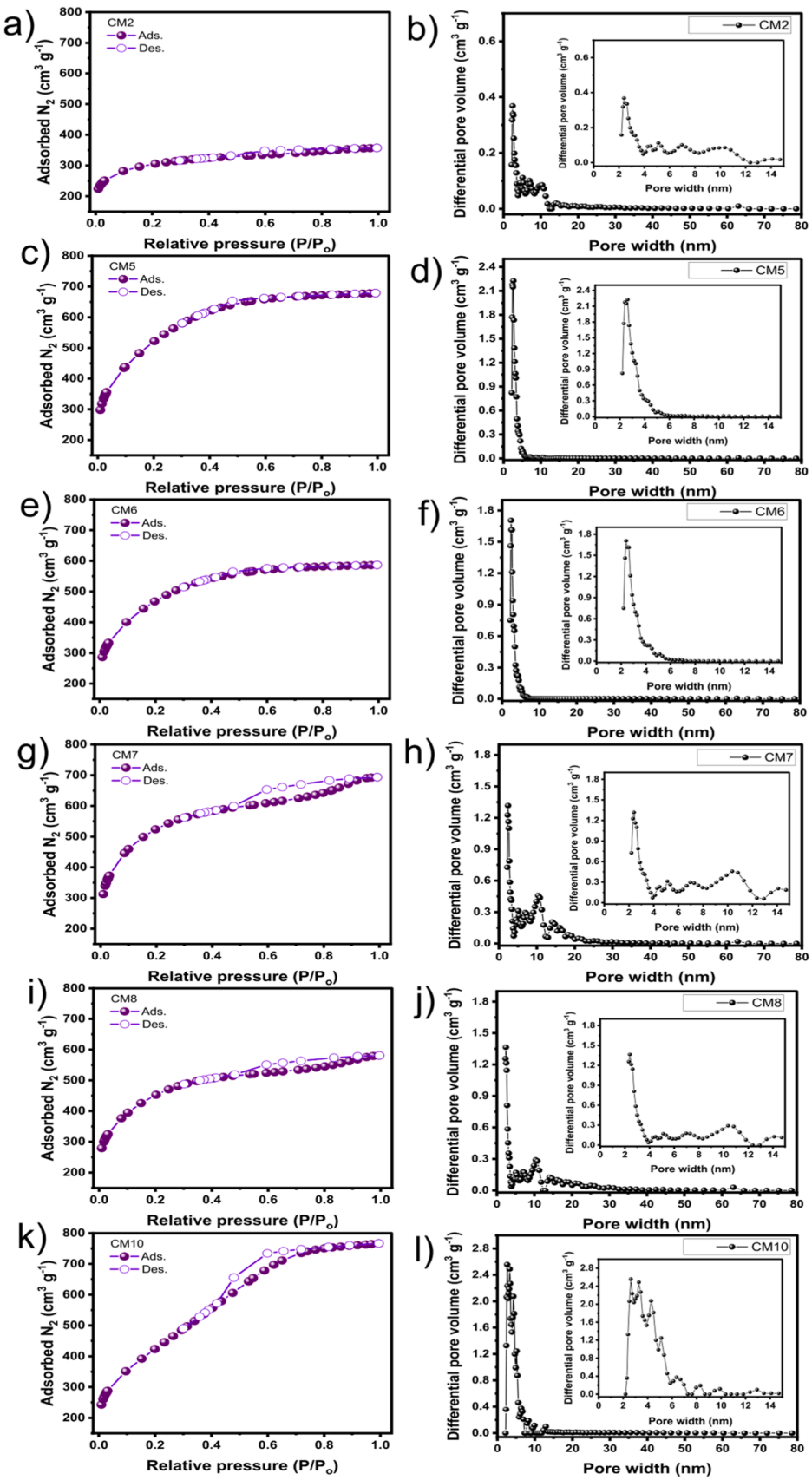

Fig. 1. Nitrogen adsorption/desorption isotherms: a) CM2, c) CM5, e) CM6, g) CM7, i) CM8 and k) CM10; and pore size distribution curves b) CM2, d) CM5, f) CM6, h) CM7, j) CM8 and l) CM10.

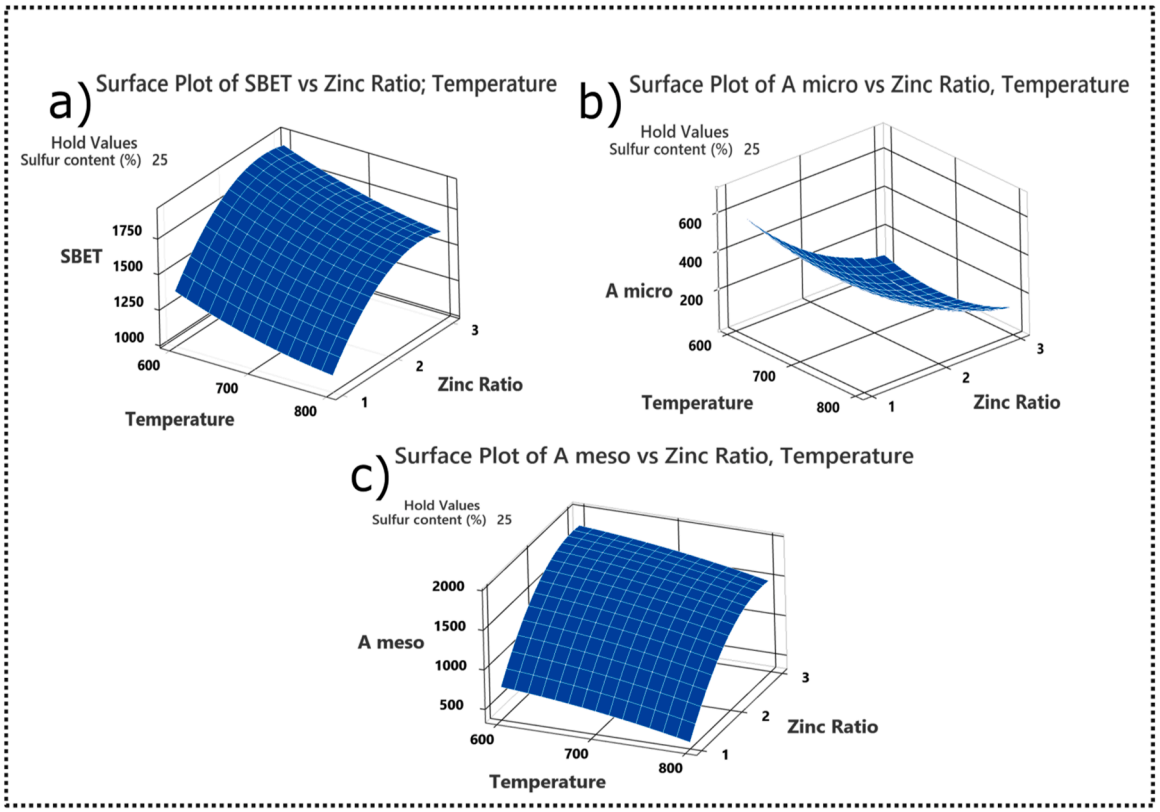

Fig. 2. Surface plots for the Box-Behken design of experiments. (a) S_{BET}, (b) A_{micro}, (c) A_{meso}.

[4–6]. Nitrogen adsorption–desorption isotherms of six samples (CM2, CM5, CM6, CM7, CM8 and CM10) were performed and are presented in Fig. 1. According to IUPAC (International Union of Pure and Applied Chemistry), the N_2 isotherms for CM2, CM5 and CM6 are similar and are close to type I [3–5], as the N_2 uptake increases at low partial pressures due to the high presence of micropores. Therefore, the CM2, CM5 and CM6 are basically microporous materials. However, a small hysteresis was observed in these three materials (empty circle, des.), which is typical of a mesoporous material, indicating a presence of some mesopores in the CM2, CM5 and CM6 materials structure, respectively. On the other hand, CM7, CM8 and CM10 have more similar curves compared to CM2, CM5 and CM6 materials whereas CM7, CM8 and CM10 exhibit more obvious hysteresis which is a signal of more mesoporous contribution [3–5]. However, the CM7, CM8 and CM10 also exhibited high N_2 uptake increases at low partial pressure, which indicate elevated presence of micropores. Overall, all carbons seemed to have a combination of micro and meso pores in their structure, as widely reported in the literature [3–5].

The pore structure of the chosen materials have been further studied by the pore size distribution curves (see Fig. 1). The six samples contain abundant micropores with a pore diameter nearly 1.85 nm. All samples contained basically big micropores and mesopores (ranging from 2.0 nm to 20 nm). These results seem to be in agreement with the results reported by the N_2 adsorption isotherms.

One of the most essential characteristics of carbonaceous materials is their porosity features, including the specific surface area and the amount of micro and mesopores. These characteristics usually significantly influence the materials' performances in adsorbing pollutants or storing energy. Table 1 shows the porosity data related to S_{BET}, A_{MESO}, A_{MICRO} and yield (in mass) of the prepared CMs. Regardless of experimental conditions, all carbons displayed high S_{BET} values(Table 1). The highest S_{BET} among the fifteen CMs was 1925 $m^2\ g^{-1}$, which was found for the sample prepared at 600 °C, a ratio of $ZnCl_2$/ Birch of 3-to-1, and 25% of S. The second highest S_{BET} was obtained for the sample prepared at 600 °C, a ratio of $ZnCl_2$/ Birch of 3-to-1, and 50% of S (1906 $m^2\ g^{-1}$).

Moreover, Table 1 shows that several other CMs exhibited S_{BET} values above 1500 $m^2\ g^{-1}$, suggesting that both using birch tree waste and the experimental setup used in the work result in an efficient strategy when aiming at producing carbon materials with very high specific surface areas. Earlier dos Reis *et al.* [5] employed a DoE to explore spruce bark as a carbon precursor to produce CMs. The CMs were also chemically activated with $ZnCl_2$. Similar pyrolysis conditions were employed, and the surface area values ranged from 739 to 1374 $m^2\ g^{-1}$, considerably lower than the CMs prepared in this work (1069–1925 $m^2\ g^{-1}$).

Besides a high total surface area, the CMs exhibited different pore structures with predominant mesoporosity. This property is highly desired in CMs that are to be used in the adsorption of organic pollutants and energy storage applications. The mesoporosity facilitates the liquid transport throughout the CM bulk and ensures enough space to adsorb/accommodate the pollutants and enable electrolyte transport and charge storage when employed as an anode in battery applications.

The mesoporosity of the CMs is attributed to the $ZnCl_2$ impregnation, which is a well-known agent for developing the mesoporosity of CMs [5, 24]. Danish *et al.* [25] employed waste wood to produce a $ZnCl_2$-impregnated carbon material with an S_{BET} of 1767 $m^2\ g^{-1}$. 95% of this total area was observed to consist of mesoporous structures.

It is reported that adding a small amount of $ZnCl_2$ is beneficial when aiming at the creation of micropores, while by increasing the $ZnCl_2$ quantity, the micropores collapse, widening in size and forming into mesopores [5,26]. Observing Table 1, the same mechanism is shown in the present study. The as prepared samples with lower $ZnCl_2$ amount (ratio of 1) exhibited higher micropore contents (CM1, CM2, CM9, and CM11), while the three carbons with the highest A_{Mseso} (CM3, CM10, and CM12) were impregnated with the higher $ZnCl_2$ amount (ratio of 3-to-1).

Table 1 A_{BET} and A_{Meso} values varied randomly regarding the preparation method in which it was imposed. By only evaluating Table 1, it is

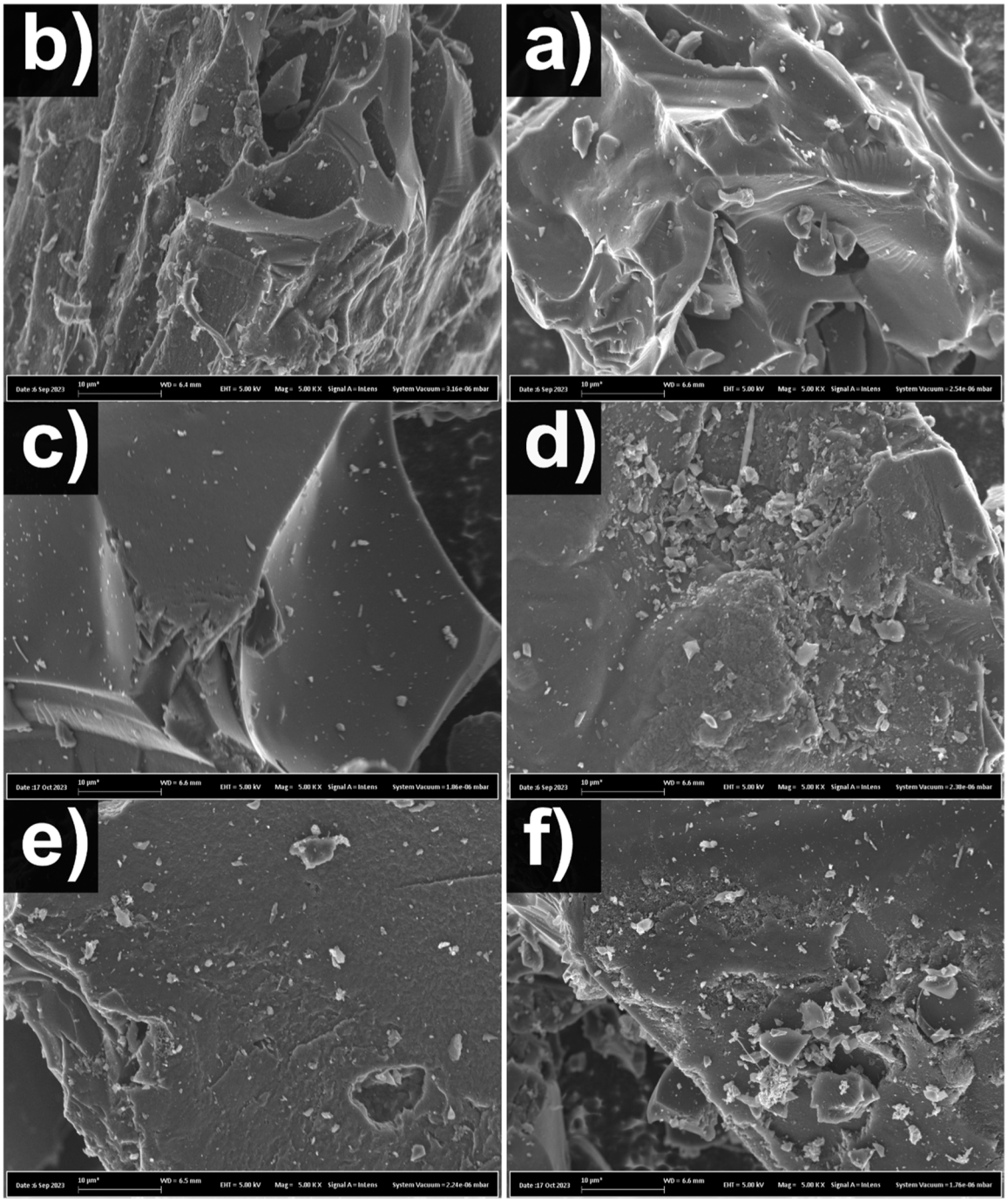

Fig. 3. SEM morphological images of CM samples: a) CM2, b) CM5, c) CM6, d) CM7, e) Cm8 and f) CM10.

impossible to establish an accurate correlation between S_{BET} and/or A_{Meso} and the factors used to prepare the CMs. However, using DoE analysis facilitates interpretation. Therefore, in the next section, DoE data analysis was employed to identify significant correlations between the chosen factors on S_{BET} and A_{Meso}.

3.2. Design of experiments for the identification and optimization process factors

The response surface regressions were presented as S_{BET} versus the temperature; Zinc Ratio; Sulfur content (%) (Table S2); Response Surface Regression: A micro versus Temperature; Zinc ratio; Sulfur content (%) (Table S3); Response Surface Regression: A meso versus Temperature; Zinc ratio; Sulfur content (%) (Table S4). All parameters with a probability of ≤ 0.05 (95% confidence level) are significant, and all parameters with a probability of > 0.05 are not significant. For the response S_{BET} (Table S2), the significant factors were the pyrolysis temperature ($p= 0.014$), $ZnCl_2$ ratio ($p= 0.001$) and the quadratic zinc ratio ($p= 0.013$). For the response area of micropores (Table S3), only the $ZnCl_2$ ratio presented a probability of < 0.005 ($p= 0.001$). For the response area of mesopores (Table S4), the $ZnCl_2$ ratio ($p= 0.000$) and quadratic $ZnCl_2$ ratio ($p= 0.021$) were significant. Notably, the sulfur content gave rise to no significant importance in all three model responses. The responses are mainly explained by the pyrolysis temperature and the $ZnCl_2$ ratio. Another critical feature observed is that two of the independent factors did not interact ($p > 0.05$). Also, from the results

Table 2 –
Elemental composition (wt%) of the CM samples.

	Carbon (%)	Hydrogen (%)	Oxygen (%)	Sulfur (%)
CM1	88.4	0.91	2.72	3.75
CM2	90.3	0.61	3.21	1.74
CM3	87.3	1.23	3.32	5.06
CM4	89.5	0.83	1.54	4.29
CM5	91.3	1.50	3.05	0.15
CM6	92.9	0.68	1.88	0.31
CM7	84.7	1.20	3.25	7.33
CM8	87.1	0.51	1.62	6.69
CM9	90.2	1.08	3.76	0.65
CM10	88.1	0.96	1.88	0.37
CM11	87.6	0.92	5.37	3.32
CM12	87.6	0.81	2.08	4.69
CM13	88.4	1.51	3.20	2.03
CM14	89.0	0.86	2.14	4.57
CM15	87.4	0.86	2.98	4.67

represented in Tables S2, S3 and S4, it is possible to infer if the increase of one parameter increases or decreases a response by observing the values of the fitted coefficients in the fitted model. When the coefficient is positive, an increase in the factor increases the response; when the coefficient has a negative value, an increase in the factor decreases the response.

The plots of the main influence for S_{BET} (Fig S1), A_{micro} (Fig S2), and A_{meso} (Fig S3) were shown. For $S_{BET,}$ it is evident that an increase in the pyrolysis temperature decreases the response (S_{BET}) significantly; while an increase in the $ZnCl_2$ ratio improved the surface area, but it presented a curvature. On the other hand, the S content did not result in any remarkable differences in the S_{BET} (p= 0.360, see Table S2). For A_{micro}, only the $ZnCl_2$ amount resulted in a remarkable decrease in the response (area of micropores). For A_{meso}, only the $ZnCl_2$ ratio significantly influenced the response. These plots confirm the response surface regression in Tables S2, S3 and S4, respectively.

Fig. 2 depicts the surface plot for the response S_{BET} (Fig. 2a), A_{micro} (Fig. 2b) and A_{meso} (Fig. 2c). The higher SBET occurs for lower pyrolysis temperatures and at higher $ZnCl_2$-to-biomass ratios (Fig. 2a). The lowest A_{micro} occurs at a higher $ZnCl_2$-to-biomass ratios (Fig. 2b). On the other hand, the highest A_{meso} occurs at a higher $ZnCl_2$-to-biomass ratio (Fig. 2c). Considering the three responses (S_{BET}, A_{micro}, and A_{meso}) and having as a target the highest S_{BET}, lowest A_{micro}, and highest $A_{meso,}$ the following conditions were chosen: Temperature of 600°, $ZnCl_2$-to-biomass ratio of 2.86, and a sulfur cencentration of 26.77%. The responses estimated were S_{BET} of 1917 m^2g^{-1}, A_{micro} 92.8 1917 m^2g^{-1}, and Ameso of 1824 m^2g^{-1}. The composite desirability was 0.9483 (see Fig S4).

3.3. Physicochemical characterization of the CMs

3.3.1. SEM analysis of the CM samples

SEM analysis was carried out to evaluate the influence of sulfur doping on the morphology properties of the CMs (Fig. 3). The SEM images of CM2, CM5, CM6, CM7, CM8 and CM10. Respectively, are shown (Fig. 3). CM5 and CM6 are samples without sulfur and both exhibited seemingly smoother surfaces with no irregular structures and no apparent porosity (holes and cracks). On the other hand, the samples CM2, CM7, CM8 and CM10 were doped with sulfur and, interestingly. in all cases more rough surfaces with holes and cracks evidencing that the incorporation of sulfur influenced the morphology of the material. These differences between the non-doped and doped CMs can be related to the incorporation of S that increases the number of defects in the biochar structure/surface [27,28], which can have a positive impact on the materials' performances when applied as adsorbents and electrodes [21, 28].

3.3.2. Elemental composition and XPS of CMs

The elemental composition of the CMs in terms of carbon (C), hydrogen (H), Oxygen (O) and sulfur (S) is shown in Table 2. For a comparative result, a commercial activated carbon has approximately 88% of C, 6–7% of O, around 1% of S, 0.5% of H and 0.5% of N, and 3–4% of impurities (mineral elements or ash) [29]. The CMs exhibited high C contents varying from 84.7 to 92.9 wt%, with a higher H content than the commercial activated carbon. The reason is probably due to the fact that the biomass contains an elevated amount of C-H groups, reflecting more hydrogen in the obtained CM than commercial activated carbon. It is worth mentioning that an elevated C content reflects improved CM features because of the physicochemical characteristics of the surface, and the thermal and electrical properties of the CMs. Moreover, it can indicate a low ash content, which is good because ash often reduces both S_{BET} and the number of surface functional groups. Regarding the samples doped with sulfur, it is worth pointing out that these samples exhibited elevated S contents, indicating a successful incorporation of it into the carbon matrix. As previously mentioned, high S content can be highly beneficial for the uptake of water contaminants and for improving the CM electrochemical performances.

The surface chemistry and elemental composition of the CM samples were further investigated by XPS in order to observe the impact of the S-doping on the carbon surface composition/functionality. The XPS survey spectra (Fig. 4) revealed an obvious presence of C and O in CM5 and CM10 (non-doped materials), while in the other samples, S was also observed, suggesting the successful incorporation of sulfur atoms in the CM structures.

Since the sulfur was detected only in S-doped CM samples, its S 2p spectra was deconvoluted and four peaks (see Fig. S5) were identified. The sulfur states are related to thiophene (C− S−C, 164.1–164.2 eV), sulfoxide (C−SO−C, 165.3–165.4 eV), sulfone (167.7–167.9 eV), and sulfate states (169.1–169.3 eV). The peak intensity of C–S–C bonds (thiophene) suggests that covalent carbon-sulfur-carbon bonds are the predominant sulfur oxidation states in the doped samples. Li *et al.*, [30] doped carbon materials for electrochemical applications (battery) and when XPS was employed to evaluate the level of doping, the S-doping ratios reached 7.1 at%, indicating the fact that the S atom replaces the C atom and O-containing groups in the carbon materials. In addition, the same sulfur states thiophene, sulfoxide, sulfone, and sulfate were detected. These sulfur states indicate an abundance of functional groups that can boost both the adsorptive and energy storage performances of the CMs [4,21].

3.3.3. Raman analysis and graphitization degree of the CM

The graphitization degree of a carbonaceous material is important because the presence of crystalline graphitic or defects could have implications in the material application. The graphitization degree is generally studied through Raman spectroscopy. As assumed in this technique, two prominent bands at around 1500–1650 cm^{-1} (G band) that are related to in-plane stretching vibration of the sp^2 hybridized carbon atoms (planar carbon structure) and a second band near 1300 cm^{-1} (D band) appears that is attributed to the sp^3 C atoms (tetrahedral carbon structure), and whose presence in the CM leads to some defects in the carbon framework [31,32]. A ratio for the I_D/I_G can be obtained from these peaks, reflecting the degree of graphitization of the CMs [3,6,31]. Fig. 5 shows the values for the I_D/I_G for all CMs. It can be seen that the I_D/I_G values are higher than 1, evidencing the presence of more defects than graphitic structure, which is typical for pyrolyzed biomass. This result indicates that the experimental preparation conditions, impregnation with $ZnCl_2$ and S-doping generated CMs with rich defective active sites that could help boost the material's adsorptive properties and electrolyte penetration into the carbon structure [21,33]. It is reported that the graphitization degree of a biomass-based carbon could be easily regulated by activation parameters, such as the type of activating agent, the ratio of biomass to the activating agent, the activation temperature and heating time [34]. In one study, Gao *et al.*, [35]

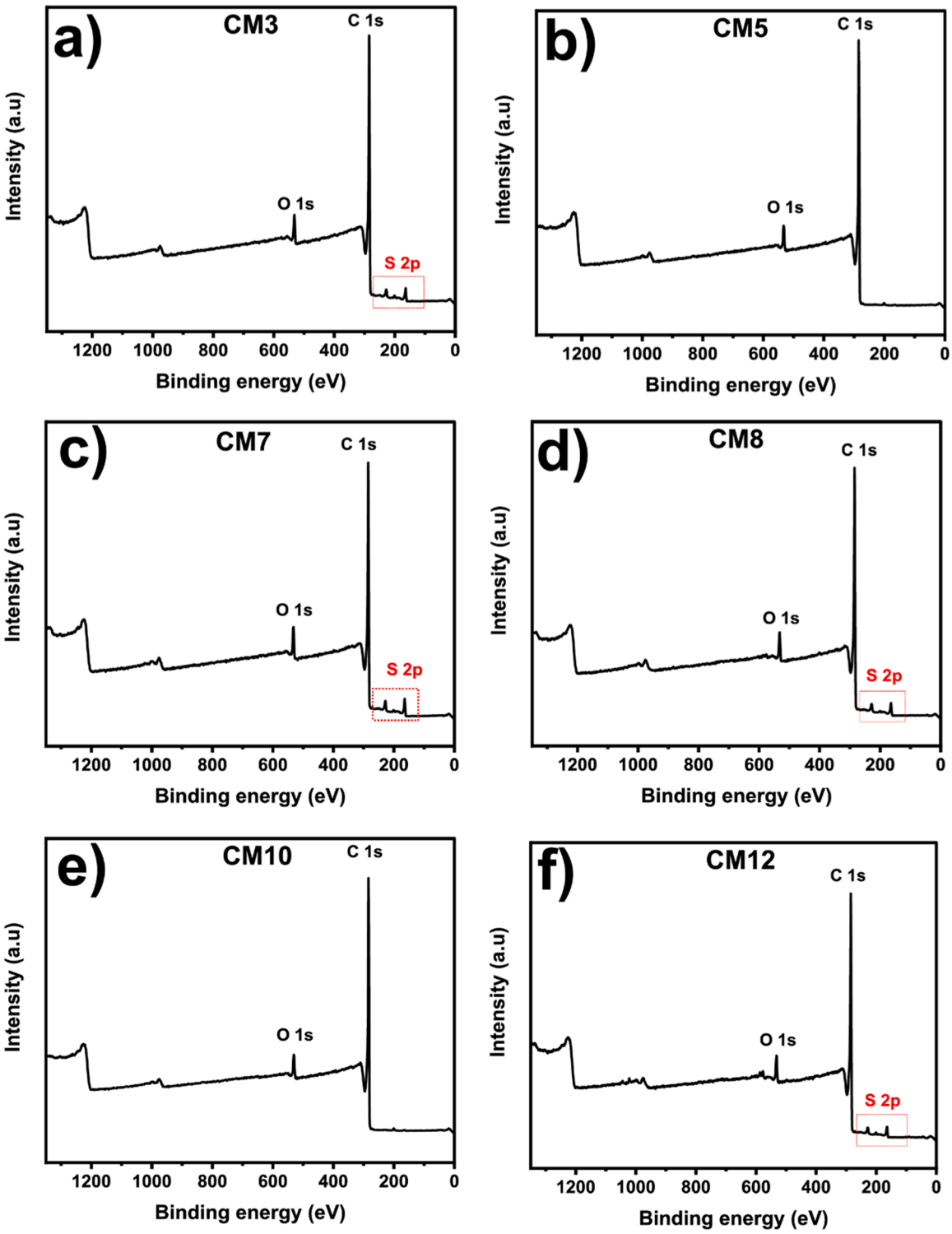

Fig. 4. XPS survey spectra of CM samples: a) CM3, b) CM5, c) CM7, d) CM8, e) CM10, and f) CM12.

prepared a butterfly-wing-derived carbon (BWCF) and uniformly grew Co–Ni–Se nanosheets on BWCF structure (Co–Ni–Se/BWCF). This method improved the graphitization degree of the carbon electrode. However, Xu *et al.*, [36] reported that the introduction of heteroatom into the carbon structure creates defects on carbon lattices, which is favorable for enhancing the capacitive contribution for energy storage of the carbon materials when used as an anode in batteries.

3.3.4. *Hydrophobicity / hydrophilicity tests of the CM samples*

Fig. 6 shows the n-heptane/water adsorption results for all CMs. From n-heptane/water adsorption data, it is possible to extract valuable information regarding hydrophobicity/hydrophilicity index (HI), indicating whether the material's surface has more hydrophobic or hydrophilic features [5,37]. According to Fig. 6 below, only 5 out of 15 CM presented a value of HI < 1 (CM2, CM6, CM9, CM11, and CM13), indicating a predominant hydrophilic behaviour. All other CM samples were observed to have a value of HI > 1, which confers a higher

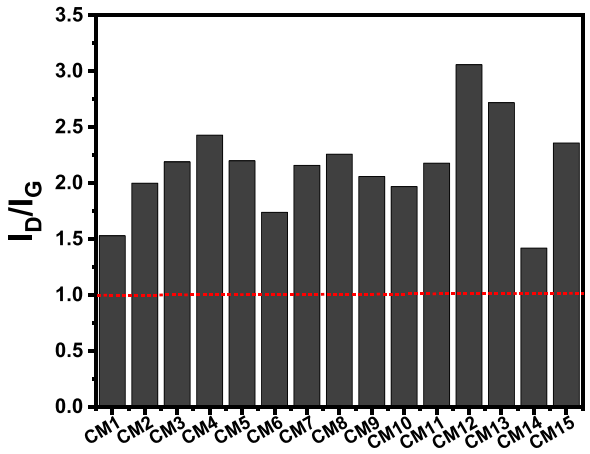

Fig. 5. Ratio of I_D/I_G bands of the CM samples.

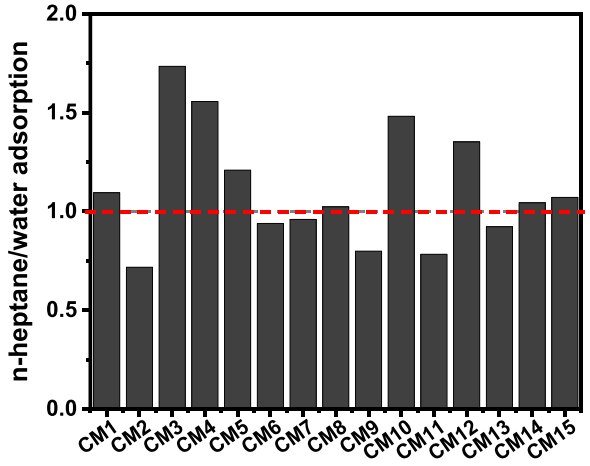

Fig. 6. – Hydrophobicity/hidrophilicity analysis (ratio between n-heptane/water vapours).

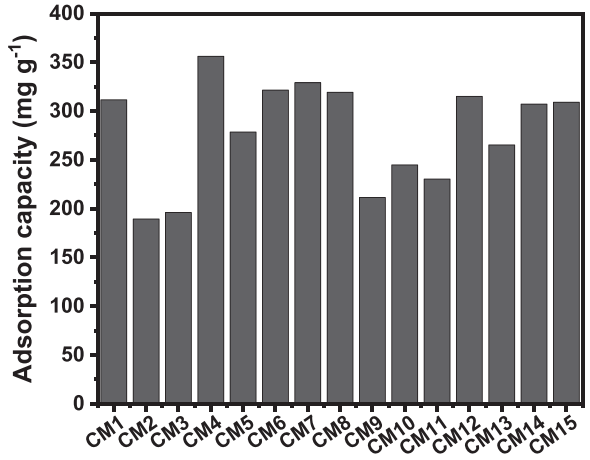

Fig. 7. - Adsorption of DCF of CMs.

hydrophobicity behaviour. The higher number of polar groups on the surface of CMs leads to a lower HI value. Conversely, CMs with fewer functional groups often are observedd to have higher HI values [5,38,39].

3.4. Environmental and electrochemical application of the CMs

3.4.1. Preliminary results on Adsorption of DCF

In order to evaluate the potential application of the CMs as adsorbents for pollutant removal, they were employed in removing DCF from aqueous solutions. Fig. 7 shows that all CMs exhibited high adsorption capacity (190 – 356 mg g^{-1}). These high adsorption capacities could be explained by the physicochemical features of the CMs, such as high surface areas and well-developed mesoporosity. To compare the adsorption results with some literature, Leite *et al.* [40] prepared seven biochars using avocado seeds as a precursor with S_{BET} ranging from 1122 to 1584 m^2 g^{-1}, and when applied as adsorbents for DCF removal, they had high uptake levels (121 – 132 mg g^{-1}); values substantially lower than the results obtained in this work. In an another work [41], graphene oxide nanosheets (GON) were employed in the adsorption of DCF, and an adsorption capacity of 128.75 mg g^{-1} was reached. GON is considered a more complex technical material associated with a high-cost synthesis, and even so, our CMs, with a more sustainable synthesis approach, presented more efficient uptake levels for DCF. These results suggest that CMs are promising candidates for removing pollutants from aqueous solutions.

The results above suggest that the prepared CMs can be effectively employed as adsorbents, one of many CMs uses. However, another potential use for these materials is as anode materials for energy storage devices such as lithium-ion batteries which is evaluated next.

3.4.2. Preliminary results on Lithium ion battery application of the CMs

The environmental suitability application of the CM samples was assessed by their adsorptive behaviour/results. In this section, the feasibility of CMs as anodes for LIBs was examined in a half-cell configuration against Li metal cycled between 0.001 and 3 V, respectively. Fig. 8 illustrates the first five charge−discharge curves for the tested anodes (CM2, CM5, CM9, CM12, CM13). The long sloping plateau under 1 V, observed at the first discharge cycle corresponds to the different phenomena such as Li^+ intercalation into the graphitic structure present in the CMs, chemical reactions between electrolyte and CMs' surface functionalities (including sulfur), and the formation of a solid–electrolyte interface (SEI) layer, resulting in a much higher first discharge capacity for all CM samples. After the first cycle, no significant change was observed during cycling due to the SEI formation and its gradual stabilization, which reduces the surface reactions, and the anodes became more chemically stable [42].

It is difficult to conclude that sulfur doping positively infleunced the electrochemical responses of the CM anodes since the current data show that the best and worst anode performances were obtained for the doped CM samples. However, our samples have shown competitive performances compared to other anode materials found in the literature [43–49] (see Table 3).

For instance, nickel/niobium tungsten oxide nanowires [43] gave rise to a smaller capacity compared to CM2 and CM9 in the first cycle, and their capacity at the 50th cycle was inferior to that of the capacity of CM2 and CM2 at the 5th cycle. It is worth pointing out that - nickel/-niobium tungsten oxide nanowires have a much more complex synthesis process, which implies higher production costs when compared to the CMs anode systems. The same logic is applied to tellurium nanoparticle/TeO_2- V_2O_5-Al_2O_3 glass anode [48] and others exhibited in Table 3. Therefore, considering the low complexity of the CM synthesis and its respective electrochemical performances, the CM samples can be considered suitable candidates in LIB anode fabrication with interesting performances.

4. Conclusions

A potential recycling method of birch wastes for the development of sulfur-doped carbon materials for environmental and energy storage applications was supported by a statistical analysis. The influencial

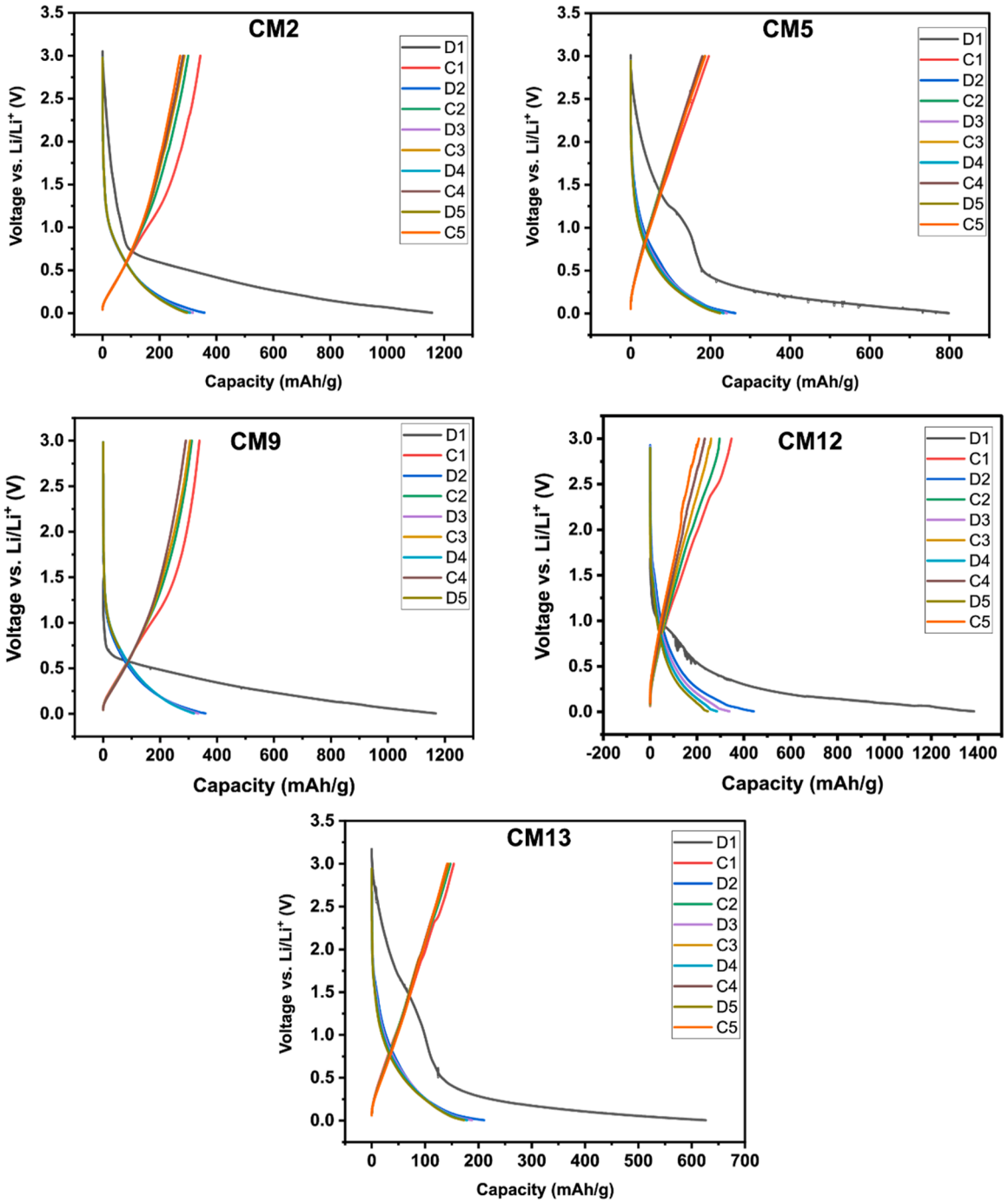

Fig. 8. First five charge–discharge cycles of CM2, CM5, CM9, CM12,CM13 anodes.

parameters were optimized through the Box-Behnken method of a robust design to make sustainable biomass-derived carbon materials. The investigated factors were the activation temperature and the $ZnCl_2$-to-biomass impregnation ratio, and sulfur content. The prepared CM materials displayed very high specific surface areas ranging from 1069 to 1925 $m^2\ g^{-1}$, larger than many reports found in the literature. The sulfur doping incorporated up to 7.33 wt% of sulfur in the CM structure, which yielded CMs with more defects and hydrophilic surfaces. According to the statistical analysis, under the studied conditions, the responses were mainly influenced by the pyrolysis temperature and the $ZnCl_2$-to biomas ratio, while the sulfur content did not result in any remarkable differences in the selected responses. However, although the sulfur doping was not critical, statistically, on the pororisy of the CMs, the morphology and the surface chemicistry of the sulfur doped CMs were impacted by the sulfur incorporation. When tested as adsorbents, CMs exhibited a very high adsorption capacity (190 – 356 mg g^{-1}), and as anodes, they showed competitive lithium charge storage capacity during the first 5 cycles (306 $mAhg^{-1}$ at 1 C for CM9). Although a small mumber of cycles, we successfully showed that such results were shown to be competitive with some reports found in the international literature.This systematic research has effectivelly provided a path to successfully produce and optimize design the suitable biomass-derived carbon materials with a high surface area and different pore structures. The conversion of birch wastes as an effective precursor into CMs also provided a comprehensive solution to both waste management and porous carbon needs.

Table 3
Comparative electrochemical performance of CM samples and other anodes for LIBs.

Anode materials	Anode synthesis method	Capacity (mA h g^{-1}) and cycle	Current density	Ref.
Nickel/Niobium tungsten oxide nanowires	Electrospinning technique followed by annealing at 900 ∘C for 6 h in air	275, 1th cycle 271, 50th cycle	0.5 C	[43]
SiO_2 nanotubes	Sol-gel and precipitation methods	625.5, 1th cycle 310, 2th cycle 239, 50th cycle		[44]
SiO_2/C	Hydrothermal reactions followed by calcination at 550 °C for 5 h (1 °C/ min)	116, 6th cycle	200 mA g^{-1}	[45]
3-dimensional SiO2/C	Hydrothermal method followed by pyrolysis (600 °C for 1 h, 3 °C per min)	312, 6th cycle	200 mA g^{-1}	[45]
Activated carbon from banana peel	Pyprolysis with KOH activation	200, 10th cycle	100 mA g^{-1}	[46]
Avocado seeds activated carbon	Pyrolysis at 750 °C for 2 h, (10 °C per min)	415, 1th cycle 355, 5th cycle		[47]
Nano-plated graphene	Sigma-Aldrich	340, 1th cycle 245, 5th cycle		[47]
Tellurium nanoparticle/ TeO_2- V_2O_5- Al_2O_3 glass		135, 1th cycle 102, 10th cycle	1000 mA g^{-1}	[48]
Apple wastes	Pyrolysis at 800 °C for 2 h, (10 °C per min); KOH activation	320, 2th cycle 240, 10th cycle	0.33 C	[49]
CM2	One-step pyrolysis at 800 °C for 1 h doped with sulfur	357, 2th cycle 298, 5th cycle	0.5 C	This work
CM9	One-step pyrolysis	360, 2th cycle 306, 5th cycle	0.5 C	This work

5. Challenges and future perspectives

This research highlights a few challenges and research directions related to heteroatom-doped porous carbon in energy storage and adsorption applications. We must point out that there is a rare coverage on comparative studies of energy storage devices (e.g., batteries) and adsorption capacity as well of similar porous carbon material modified by different heteroatoms or the different porous carbon materials doped with the same heteroatom (sulfur), which makes it challenging to understand the influence of sulfur doping on the porous carbon materials in a deeper level. (i) Difficulties in controlling and understanding the pore geometry and pore size when involving chemical activators and sulfur doping processes to obtain carbon materials with suitable S_{BET} and porous structure for the desired end application. (ii) Poor information on basic principles (fundamental understanding) of the mechanisms and the influence of sulfur doping methods on the surface area, pore size, and surface chemistry connected to the biomass-derived carbon materials battery and adsorption performances. A much deeper study evaluating all synergic parameters influencing the level of doping on the physicochemical features of the doped-carbon materials such as pyrolysis temperature, pyrolysis time, chemical and physical activation, ratio of heteroatom. (iii) Difficulties in choosing biomass precursors to significantly influence the efficiency of the heteroatom-doping in terms of boosting the biomass-based carbon properties suitable for each end application (like batteries and adsorption) such as enhancing the graphitization degree or controlling the degree of defects, enhancing the S_{BET} (that has positive impact on adsorption but generally not a desired impact in LIBs), expanding carbon interlayer spacing and etc. Therefore, a deeper study on tailoring the doping process (with a specific heteroatom, e.g., sulfur) to target battery application or upon removal of specific contaminants is needed. Also as a future work, the full electrochemical tests of the CMs will be conducted for lithium-ion and sodium-ion batteries.

CRediT authorship contribution statement

Eder Claudio Lima: Writing – review & editing, Data curation. **Tao Hu:** Writing – review & editing, Formal analysis. **Mikael Thyrel:** Writing – review & editing. **Jyri-Pekka Mikkola:** Writing – review & editing, Data curation. **Shaikshavali Petnikota:** Methodology, Formal analysis. **Gopinathan Manavalan:** Methodology, Formal analysis. **Julie Thivet:** Writing – original draft, Methodology, Investigation, Formal analysis. **Ewen Laisné:** Writing – original draft, Methodology, Investigation. **Glaydson Simões dos Reis:** Writing – original draft, Supervision, Project administration, Methodology, Formal analysis, Data curation, Conceptualization. **Ulla Lassi:** Writing – review & editing, Funding acquisition. **Mu. Naushad:** Writing – review & editing.

Declaration of Competing Interest

The authors declare the following financial interests/personal relationships which may be considered as potential competing interests: Glaydson Simoes dos Reis reports financial support was provided by Swedish University of Agricultural Sciences. If there are other authors, they declare that they have no known competing financial interests or personal relationships that could have appeared to influence the work reported in this paper.

Data Availability

Data will be made available on request.

Acknowledgements

The authors wish to thank Bio4Energy, a strategic research environment appointed by the Swedish government, as well as the Swedish University of Agricultural Sciences for supporting this work. EU/Interreg Aurora (Project GreenBattery, grant no 20357605) and KEMPE Foundations are gratefully acknowledged for funding. Wallenberg Wood Science Center under auspices of Alice and Knut Wallenberg Foundation are gratefully acknowledged. This work is also a part of the activities of the Johan Gadolin Process Chemistry Centre at Åbo Akademi University. The Umeå Core Facility for Electron Microscopy (UCEM-NMI node) and the Vibrational Spectroscopy Core Facility (ViSp) at the Chemical Biological Centre (KBC), Umeå University, are acknowledged. The authors wish to thank A. Gorzsas for supporting Raman measurements, and A. Shchukarev for supporting XPS measurements. The authors thank CNPq, FINEP, and CAPES from Brazil for partially supporting this research. In addition, the authors are also grateful to the Researchers Supporting Project number (RSP2024R8), King Saud University, Riyadh, Saudi Arabia, for the financial support.

Appendix A. Supporting information

Supplementary data associated with this article can be found in the online version at doi:10.1016/j.colsurfa.2024.133899.

References

[1] M. Casau, M.F. Dias, J.C.O. Matias, L.J.R. Nunes, Residual biomass: a comprehensive review on the importance, uses and potential in a circular bioeconomy approach, Resources 11 (2022) 35.

[2] H.A. Murillo, L.A. Díaz-Robles, R.E. Santander, F.A. Cubillos, Conversion of residual biomass into valuable biofuels by co-hydrothermal carbonization for utilization in household pellet stoves, Biomass Bioenergy 151 (2021) 106153.

[3] G.S. dos Reis et al., Synthesis of novel mesoporous selenium-doped biochar with high-performance sodium diclofenac and reactive orange 16 dye removals, Chemical Engineering Science, https://doi.org/10.1016/j.ces.2023.119129.

[4] M. Gonzalez-Hourcade, G.S. dos Reis, A. Grimm, V.M. Dinh, E.C. Lima, S. H. Larsson, F.G. Gentili, Microalgae biomass as a sustainable precursor to produce nitrogen-doped biochar for efficient removal of emerging pollutants from aqueous media, J. Clean. Prod. 348 (2022) 131280.

[5] G.S. dos Reis, S.H. Larsson, M. Thyrel, M. Mathieu, P.N. Tung, Application of design of experiments (DoE) for optimized production of micro-and mesoporous Norway spruce bark activated carbons, Biomass-.-. Conv. Bioref. 13 (2023) 10113–10131, https://doi.org/10.1007/s13399-021-01917-9.

[6] G.S. dos Reis, D. Bergna, A. Grimm, E.C. Lima, T. Hu, Mu Naushad, U. Lassi, Preparation of highly porous nitrogen-doped biochar derived from birch tree wastes with superior dye removal performance, Colloids Surf. A Physicochem. Eng. Asp. 669 (2023).

[7] G.S. dos Reis, R.A.P. Lima, S.H. Larsson, C.M. Subramaniyam, V.M. Dinh, M. Thyrel, H.P. de Oliveira, Flexible supercapacitors of biomass-based activated carbon-polypyrrole on eggshell membranes, J. Environ. Chem. Eng. 9 (2021) 106155.

[8] Y. Xue, X. Guo, M. Wu, J. Chen, M. Duan, J. Shi, J. Zhang, F. Cao, Y. Liu, Q. Kong, Zephyranthes-like Co2NiSe4 arrays grown on 3D porous carbon frame-work as electrodes for advanced supercapacitors and sodium-ion batteries, Nano Res. 14 (2021) 3598–3607.

[9] K. Nuithitikul, S. Srikhun, S. Hirunpraditkoon, Influences of pyrolysis condition and acid treatment on properties of durian peel-based activated carbon, Bioresour. Technol. 101 (2010) 426–429.

[10] A. Budianto, E. Kusdarini, N.H. Amrullah, E. Ningsih, K. Udyani, A. Aidawiyah, Physics and chemical activation to produce activated carbon from empty palm oil bunches waste, IOP Conf. Ser.: Mater. Sci. Eng. 1010 012016.

[11] F. Amrana, M.A.A. Zaini, Effects of chemical activating agents on physical properties of activated carbons – a commentary, Water Pract. Technol. 15 (2020) 863–876.

[12] G.S. Dos Reis, D. Bergna, S. Tuomikoski, A. Grimm, E.C. Lima, M. Thyrel, N. Skoglund, U. Lassi, S.H. Larsson, Preparation and characterization of pulp and paper mill sludge-activated biochars using alkaline activation: a box–behnken design approach, ACS Omega 7 (36) (2022) 32620–32630.

[13] Steven A. Weissman, Neal G. Anderson, Design of experiments (DoE) and process optimization. a review of recent publications, Org. Process Res. Dev. 19 (2015) 1605–1633.

[14] S. Pradhan, M. Shahbaz, A. Abdelaal, T. Al-Ansari, H.R. Mackey, G. McKay, Optimization of process and properties of biochar from cabbage waste by response surface methodology, Biomass Convers. Bioref. 12 (2022) 5479–5491.

[15] Sabolc Pap, Paul P.J. Gaffney, Qunying Zhao, Daniela Klein, Yuan Li, Caroline Kirk, Mark A. Taggart, Optimizing production of a biochar made from conifer brash and investigation of its potential for phosphate and ammonia removal, Ind. Crops Prod. 185 (2022) 115–165.

[16] M.K.B. Gratuito, T. Panyathanmaporn, R.-A. Chumnanklang, N. Sirinuntawittaya, A. Dutta, Production of activated carbon from coconut shell: optimization using response surface methodology, Biores. Technol. 99 (2008) 4887–4895.

[17] Mohammad Umair Jamal, Ashleigh J. Fletcher, Design of Experiments Study on Scottish Wood Biochars and Process Parameter Infuence on Final Biochar Characteristics, BioEnergy Research https://doi.org/10.1007/s12155-023-10595-6.

[18] A.N. Kislitsyn, Birch bark extractives: isolation composition, properties, application, Khim. Drev. 3 (1994) 3–28.

[19] H. Dubois, E. Verkasalo, H. Claessens, Potential of birch (Betula pendula Roth and B. pubescens Ehrh.) for forestry and forest-based industry sector within the changing climatic and socio-economic context of Western Europe, Forests 11 (2020) 336.

[20] X. Tan, S. Liu, Y. Liu, Y. Gu, G. Zeng, X. Hu, X. Wang, S. Liu, J. Lu-hua, Biochar as potential sustainable precursors for activated carbon production: Multiple applications in environmental protection and energy storage, Bioresour. Technol. 227 (2017) 359–372.

[21] G.S. Dos Reis, H.P. de Oliveira, S.H. Larsson, M. Thyrel, E.C. Lima, A short review on the electrochemical performance of hierarchical and nitrogen-doped activated biocarbon-based electrodes for supercapacitors, Nanomaterials 11 (2021) 424.

[22] Y. Gao, Q. Wang, G. Ji, A. Li, J. Niu, Doping strategy, properties and application of heteroatom-doped ordered mesoporous carbon, RSC Adv. 11 (2021) 5361.

[23] K. Pang, W. Sun, F. Ye, L. Yang, M. Pu, C. Yang, Q. Zhang, J. Niu, Sulfur-modified chitosan derived N, S-co-doped carbon as a bifunctional material for adsorption and catalytic degradation sulfamethoxazole by persulfate, J. Hazard. Mater. 424 (2022) 127270, https://doi.org/10.1016/j.jhazmat.2021.127270.

[24] F. Cesano, S. Cravanzola, V. Brunella, D. Scarano, Porous carbon spheres from poly (4-ethylstyrene-co-divinylbenzene: role of ZnCl2 and KOH agents in affecting porosity, surface area and mechanical properties, Microporous Mesoporous Mater. 288 (2019) 10960.

[25] M. Danish, R. Hashim, M.N.M. Ibrahim, O. Sulaiman, Optimization study for preparation of activated carbon from Acacia mangium wood using phosphoric acid, Wood Sci. Technol. 48 (2014) 1069–1083.

[26] M.R. Benzigar, S.N. Talapaneni, S. Joseph, K. Ramadass, G. Singh, J. Scaranto, U. Ravon, K. Al-Bahilyc, A. Vinu, Recent advances in functionalized micro and mesoporous carbon materials: synthesis and applications, Chem. Soc. Rev. 47 (2018) 2680.

[27] Y. Zhang, J. Zhao, Comparison of different S-doped biochar materials to activate peroxymonosulfate for efficient degradation of antibiotics, Chemosphere 308 (2022) 136442.

[28] Z. Zhao, H. Chen, W. Zhang, S. Yi, H. Chen, Z. Su, B. Niu, Y. Zhang, D. Long, Defect engineering in carbon materials for electrochemical energy storage and catalytic conversion, Mater. Adv. 4 (2023) 835–867.

[29] C.R. Correa, T. Otto, A. Kruse, Infuence of the biomass components on the pore formation of activated carbon, Biomass Bioenergy 97 (2017) 53–64.

[30] Z. Li, Y. Yang, G. Ding, L. Wei, G. Yao, H. Niu, F. Zheng, Q. Chen, Optimizing the nitrogen configuration in interlayer-expanded carbon materials via sulfurbridged bonds toward remarkable energy storage performances, J. Mater. Chem. A 10 (2022) 10033.

[31] M. Pawlyta, J. Rouzaud, S. Duber, Raman microspectroscopy characterization of carbon blacks: spectral analysis and structural information, Carbon 84 (2015) 479–490.

[32] V. Piergrossi, C. Fasolato, F. Capitani, G. Monteleone, G. Postorino, P. Gislon, Application of Raman spectroscopy in chemical investigation of impregnated activated carbon spent in hydrogen sulfde removal process, Int. J. Environ. Sci. Technol. 16 (2019) 227–1238.

[33] J. Wang, Y. Qin, L. Li, S. Zhang, X. Pei, Z. Niu, X.-C. Zheng, D. Li, Defective engineering and heteroatom doping construction in carbon nanobowls for achieving high-rate potassium-ion storage with long cyclic life, Chem. Eng. J. 457 (2023) 141253.

[34] Y.W. Yap, N. Mahmed, M.N. Norizan, S.Z. Abd Rahim, M.N.A. Salimi, K.A. Razak, I. S. Mohamad, M. Abdullah, M.Y.M. Mohamad, Recent advances in synthesis of graphite from agricultural bio-waste material: a review, Materials 16 (2023) 3601.

[35] M. Gao, Y. Xue, Y. Zhang, C. Zhu, H. Yu, X. Guo, S. Sun, S. Xiong, Q. Kong, J. Zhang, Growing Co–Ni–Se nanosheets on 3D carbon frameworks as advanced dual functional electrodes for supercapacitors and sodium ion batteries, Inorg. Chem. Front. 9 (2022) 3933–3942.

[36] Y. Xu, X. Sun, Z. Li, L. Wei, G. Yao, H. Niu, Y. Yang, F. Zheng, Q. Chen, Boosting the K+ -adsorption capacity in edgenitrogen doped hierarchically porous carbon spheres for ultrastable potassium ion battery anodes, Nanoscale 13 (2021) 19634–19641.

[37] C. Lai, X.P. Gao, B. Zhang, T.Y. Yan, Z. Zhou, Synthesis and electrochemical performance of sulfur/highly porous carbon composites, J. Phys. Chem. C. 113 (2009) 4712–4716.

[38] D.R. Lima, E.C. Lima, P.S. Thue, S.L.P. Dias, F.M. Machado, M.K. Seliem, F. Sher, G. S. dos Reis, M.R. Saeb, J. Rinklebe, Comparison of acidic leaching using a conventional and ultrasound-assisted method for preparation of magneticactivated biochar, J. Environ. Chem. Eng. 9 (2021) 105865.

[39] P.S. Thue, D.R. Lima, E.C. Lima, R.A. Teixeira, G.S. dos Reis, S.L.P. Dias, F. M. Machado, Comparative studies of physicochemical and adsorptive properties of biochar materials from biomass using different zinc salts as activating agents, J. Environ. Chem. Eng. 10 (2022) 107632.

[40] A.J.B. Leite, A.C. Sophia, P.S. Thue, G.S. dos Reis, S.L.P. Dias, E.C. Lima, J.C. P. Vaghetti, F.A. Pavan, W.S. de Alencar, Activated carbon from avocado seeds for the removal of phenolic compounds from aqueous solutions, Desalin. Water Treat. 71 (2017) 168–181.

[41] A.C.S. Guerra, M.B. de Andrade, T.R.:T. dos Santos, R. Bergamasco, Adsorption of sodium diclofenac in aqueous medium using graphene oxide nanosheets, Environ. Technol. 42 (2021) 2599–2609.

[42] G.S. dos Reis, C.M. Subramaniyam, A.D. Cárdenas, S.H. Larsson, M. Thyrel, U. Lassi, F. García-Alvarado, Facile synthesis of sustainable activated biochars with different pore structures as efficient additive-carbon-free anodes for lithium- and sodium-ion batteries, ACS Omega 7 (2022) 42570–42581.

[43] B.O. Fatile, M. Pugh, M. Medraj, Nickel-doped $Nb_{18}W_{16}O_{93}$ nanowires with improved electrochemical properties for lithium-ion battery anodes, Mater. Chem. Phys. 307 (2023) 128179.

[44] J. Tang, X. Dai, F. Wu, Y. Mai, X. Wang, H. Jin, Y.Xie Yijing, A simple and efficient one-pot synthesis of SiO2 nanotubes with stable structure and controlled aspect ratios for anode materials of lithium-ion batteries, Ionics 26 (2020) 639–648.

[45] S. Suh, S. Han, H. Yoon, H. Kim, J. Kang, C. Pak, H.-J. Kim, Facile one-step fabrication of 3-Dimensional SiO2-C electrodes for lithium-ion batteries using a highly porous SBA-15 template and pore-forming agent, Electron. Mater. Lett. 18 (2022) 187–196.

[46] R.R. Gaddam, D. Yang, R. Narayan, K. Raju, N.A. Kumar, X.S. Zhao, Biomass derived carbon nanoparticle as anodes for high performance sodium and lithium ion batteries, Nano Energy 26 (2016) 346–352.

[47] T.J. Yokokura, J.R. Rodriguez, V.G. Pol, Waste biomass-derived carbon anode for enhanced lithium storage, ACS Omega 5 (2020) 19715–19720.

[48] J. Fana, Y. Zhang, G. Lia, Y. Yue, Tellurium nanoparticles enhanced electrochemical performances of TeO2- V2O5-Al2O3 glass anode for Lithium-ion batteries, J. Non-Cryst. Solids 521 (2019) 1194.

[49] C. Hernández-Rentero, V. Marangon, M. Olivares-Marín, V. Gómez-Serrano, Á. Caballero, J. Morales, J. Hassoun, Alternative lithium-ion battery using biomass-derived carbons as environmentally sustainable anode, J. Colloid Interface Sci. 573 (2020) 396–408.